IEEE Access
Multidisciplinary | Rapid Review | Open Access Journal

Received January 23, 2022, accepted March 29, 2022, date of publication April 5, 2022, date of current version April 20, 2022.

Digital Object Identifier 10.1109/ACCESS.2022.3165052

Numerical Demonstration of Angle-Independent Electromagnetic Transparency in Short-Wavelength Infrared Regime

JUNJEONG PARK, SUN K. HONG, (Senior Member, IEEE), AND HAEJUN CHUNG
School of Electrical Engineering, Soongsil University, Seoul 06978, South Korea

Corresponding author: Haejun Chung (haejun@ssu.ac.kr)

This work was supported in part by the Ministry of Science, ICT (MSIT), South Korea, under the High-Potential Individuals Global Training Program, supervised by the Institute for Information and Communications Technology Planning and Evaluation (IITP), under Grant IITP-2021-0-02125; and in part by the Soongsil University Research Fund (Convergence Research), in 2021.

ABSTRACT Realizing electromagnetic transparency in the visible light regime and beyond is an important challenge in both fundamental electromagnetics and angular-independent spectral filters for 6G communication and military applications. A conventional way of achieving electromagnetic transparency is based on Surface Plasmon Resonances (SPRs) of symmetric metallic spherical or cylindrical structures. However, symmetric objects have a constraint on their shape tunability, limiting them to visible wavelength applications. In this work, we address the limitation by designing floating nano-chips with a broken symmetry using a cluster of silver ellipsoids. We combine Bohren and Huffman analytic solutions and particle swarm optimization to accelerate the discovery of the optimum ellipsoid designs. The optimized nano-chips demonstrate clear angle-independent transparency at the 1450–1500nm wavelength window. This result is validated in full-wave Maxwell's solution via three-dimensional finite-difference time-domain method. The proposed design method can be extended to electromagnetic applications that require a design and optimization of small objects ($< \lambda/200$) compared to their operating wavelength.

INDEX TERMS Finite-difference time-domain (FDTD) method, particle swarm optimization (PSO), plasmon induced transparency.

I. INTRODUCTION

Manipulating optical response with nanostructures has been studied through multiple platforms such as metamaterials [1]–[4], metasurfaces [5]–[8], and plasmonic nanostructures [9]–[15]. Among them, achieving narrow-band electromagnetic transparency becomes attractive for both fundamental electromagnetics and angular-independent spectral filters for 6G communication and battlefield electromagnetic environment. Most studies related to achieving narrow-band electromagnetic transparency employ Extraordinary Optical Transmission (EOT) [16]–[18], plasmonic nano-particles [19], [20], and others [21]–[23]. Both EOTs and surface plasmon resonance (SPR)-based transparency show either highly angle-dependent characteristics or a limited operation band (mainly to the visible wavelength) [24]–[26]. The latter primarily utilizes symmetric objects (e.g., cylindrical or spherical symmetries [27]–[29]) for achieving angle-independent responses, which restricts a tunability regarding the resonance frequency. Therefore, realizing electromagnetic transparency in an infrared regime or beyond is still challenging.

In this work, we numerically demonstrate angle-independent electromagnetic transparency at 1450–1500nm wavelength regime through floating nano-chips in the form of a silver ellipsoid cluster attached to a SiO_2 substrate. The designing cluster of nano-particles is a particular problem in the infrared regime because an operating wavelength is much longer than the size of the nano-particles. Specifically, for 2000nm wavelength, 10-nm-radius of the ellipsoid may require a simulation grid spacing of $\Delta x \approx \lambda/200$ or less, where a typical Finite-Difference Time-Domain (FDTD) requires at least $\lambda/10$ grid spacing [30], [31] to satisfy an accuracy and numerical stability conditions [32]–[35]. This corresponds to an increase in simulation time by 20^4 (= 160,000) in 3D simulations. We propose

The associate editor coordinating the review of this manuscript and approving it for publication was Guido Lombardi.

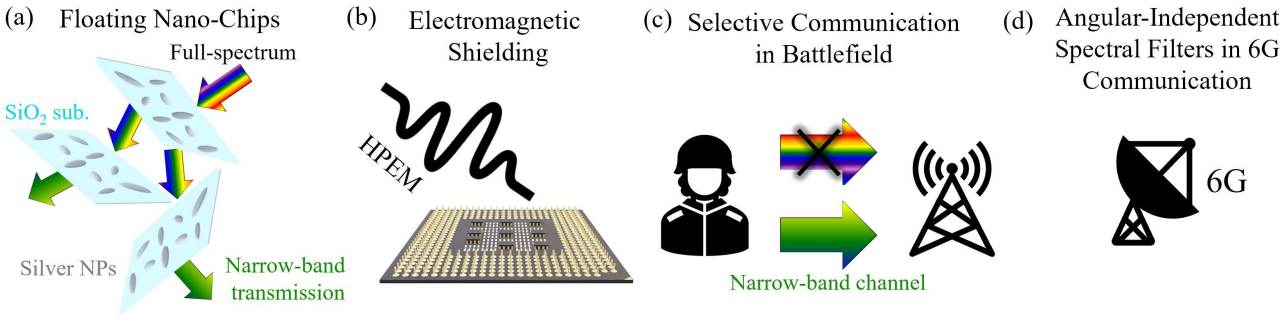

FIGURE 1. (a) A schematic diagram that demonstrates floating nano-chips enabling a selective light transmission. Incidence electromagnetic waves pass through multiple nano-chips, which filter out waves with nontarget wavelengths. Potential applications of (b) electromagnetics shielding in High-Power EM (HPEM), (c) selective communication in battlefield environment, (d) angular-independent spectral filters in 6G communications.

a novel optimization framework that combines a Particle Swarm Optimization (PSO) [36] and Bohren, Huffman's analytic solution of nano-particle scattering [37] to address this issue. The proposed method enables the design of floating nano-chips to realize angle-independent electromagnetic transparency in the infrared regime. The optimized nano-chip shows transparency between 1450–1500nm wavelength over a short-wavelength infrared regime for normal and oblique incidence waves.

Our work is written as follows: we compare and validate the absorption spectrum of silver ellipsoids in analytic prediction (BH model) and numerical calculations (FDTD). Then, we combine the BH model and PSO to determine the optimum designs of the silver ellipsoids. The optimum floating nano-chip is validated in full-wave Maxwell solution (FDTD) for normal and oblique incident waves. Finally, we assume multiple transmission events of the floating nano-chips to demonstrate electromagnetic transparency in a short-wavelength infrared regime.

II. METHOD

Typical metasurfaces for perfect absorption consist of periodic unit-cells [19], [26], [28], [38]–[43] that may suffer from wavelength and angle-dependent characteristics due to the nature of periodicity. To avoid the angle-dependent issue, symmetric objects (e.g., spheres, cylinders) have been studied for the angle-independent response of the metasurface [25], [44], [45]. However, their absorption mechanisms mostly rely on surface plasmons, where absorption peaks occur only at the resonance frequencies. As an alternative, a hybrid approach, where periodic unit cells have asymmetric rectangular-hole dimers creating Fano resonance, has been suggested [20]. This approach successfully creates two resonance peaks in the 3.54 GHz regime. In our work, we fully explore the broken symmetry of the metallic objects for achieving electromagnetic transparency in the infrared regime. A major obstacle in studying multiple nano-particle systems in an infrared regime is a computational complexity, which arose due to the considerable difference between operating wavelengths (a few thousand nanometers) and nano-particle size (few tens nanometers). This may require a simulation grid spacing around $\lambda/200$, which requires $(20)^4$ fold simulation time compared with a typical grid spacing ($\lambda/10$) used in FDTD. Optimizing those nano-particles is even more difficult, as it requires hundreds to thousands of simulations. We combine global optimization (PSO) [36] with an analytic solution (BH model) [37] of nano-particle response to address this computational issue. The BH model basically predicts the absorption and scattering of small particles in a much faster manner. We extend the use of the BH model for predicting the absorption of multiple ellipsoids and then validate it against numerical calculations. Specifically, we assume that the surface plasmon near the metallic ellipsoid may not interact significantly with neighboring ellipsoids if they have enough distance among them. This assumption will be validated with FDTD simulations [31]. We use Meep [32], an open-source software library for electromagnetics simulation via FDTD.

To validate our hypothesis, we first compare absorption spectra of different sizes of the silver ellipsoids whose long and short axes are a and b, respectively, as shown in Fig. 2. The dielectric constants of silver and SiO_2 used in this work are obtained from Ref [46]; then, we numerically model the dielectric constants using a Drude-Lorentz dispersion equation [32], [46]. The curves in Fig. 2 indicate an analytic absorption spectrum predicted by the BH model [37]; the dots mean absorption spectrum calculated by Meep. The BH model predicts absorption and scattering of each ellipsoid with given equations [37]:

$$e^2 = 1 - \frac{b^2}{a^2} \tag{1}$$

$$L_1 + L_2 + L_3 = 1 \tag{2}$$

$$L_1 = \frac{1-e^2}{e^2}\left(-1 + \frac{1}{2e}\ln\frac{1+e}{1-e}\right) \tag{3}$$

$$L_2 = \left(\frac{1-L_1}{2}\right) \tag{4}$$

$$L_3 = L_2, \tag{5}$$

where 'a' and 'b' indicate the lengths of the long and short axis of the ellipsoid, respectively. e is an eccentricity of

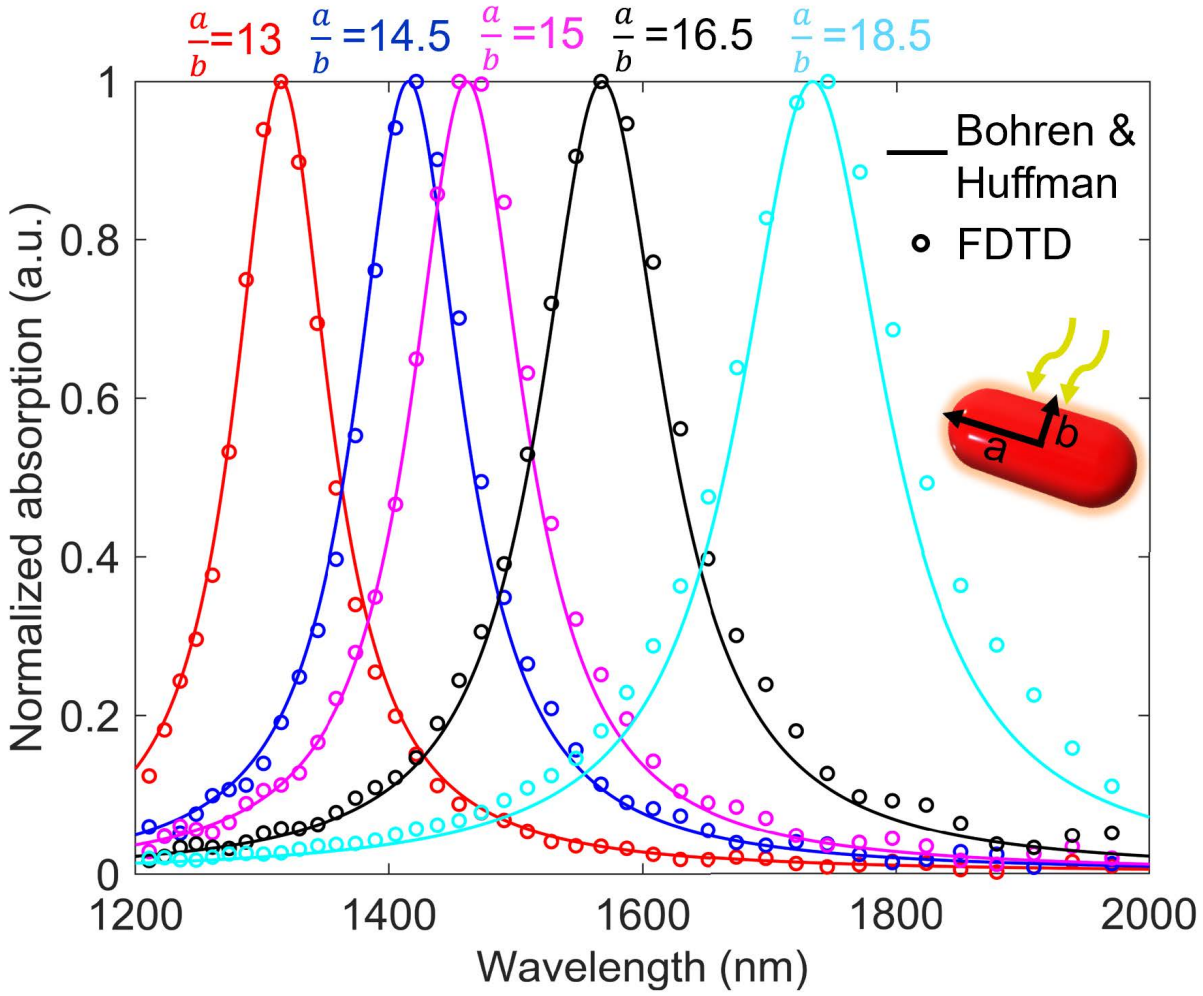

FIGURE 2. Normalized absorption calculated via Finite-Difference Time-Domain (FDTD) method (dots) and the Bohren and Huffman (BH) analytic model [37]. 'a' and 'b' indicate a long axis and a short axis of the silver ellipsoid, respectively. The absorption spectra calculated by the FDTD and the BH model are normalized against their maximum values for better visibility. The absorption spectra agree well for analytic calculation and numerical validation.

ellipsoid defined by 'a' and 'b', and also L_i is a geometrical factor defined by eccentricity. ($i = 1, 2, 3$)

$$\alpha_i = \frac{\chi}{L_i + 1} = \frac{\epsilon_r - 1}{L_i + 1}, \tag{6}$$

where α_i is the polarizability of an ellipsoid in a field parallel to each axis expressed by geometrical factor (L_i) and relative permittivity (ϵ_r).

$$V \cdot Q_{abs} = \frac{1}{3} k \mathrm{Im}\left(\alpha_1 + \alpha_2 + \alpha_3\right) \tag{7}$$

$$V \cdot Q_{scat} = \frac{4}{3}\pi a^2 b \frac{k^4}{6\pi}\left(\frac{|\alpha_1|^2}{3} + \frac{|\alpha_2|^2}{3} + \frac{|\alpha_3|^2}{3}\right), \tag{8}$$

where V is a volume of an ellipsoid, and Q_{abs}, Q_{scat} are respectively the efficiency per volume of each response defined by factors and parameters such as k, which is the wave vector.

We fix a short axis (b) as 10nm and vary a long axis (a) to validate the analytic prediction versus simulations. The comparison shows that they match well in the infrared regime, as depicted in Fig. 2. Thus, in the next step, we use the BH model to calculate the absorption spectrum in the PSO method in a much faster way. Figure 2 also shows that a combination of well-designed silver ellipsoids may create the desired absorption spectrum because the absorption peaks can fully cover our designated wavelength range. We choose PSO to explore the best possible combination of the silver ellipsoids. The fitness function ($\mathcal{F}$) of the PSO is given by

$$\mathcal{F} = \int_{\lambda_{\min}}^{\lambda_{\max}} |\{\sum_{\mathrm{n}} A_{\mathrm{BH,n}}(\lambda)\} - A_{\mathrm{tar}}(\lambda)| d\lambda, \tag{9}$$

where $\lambda_{\max}$ is 2200nm, $\lambda_{\min}$ is 1000nm, $A_{\mathrm{BH,n}}$ is an absorption spectrum of the $\mathrm{n_{th}}$ ellipsoid predicted by the BH model, A_{tar} is a target absorption spectrum which is a step function where it has zero values between 1450–1500nm while it has

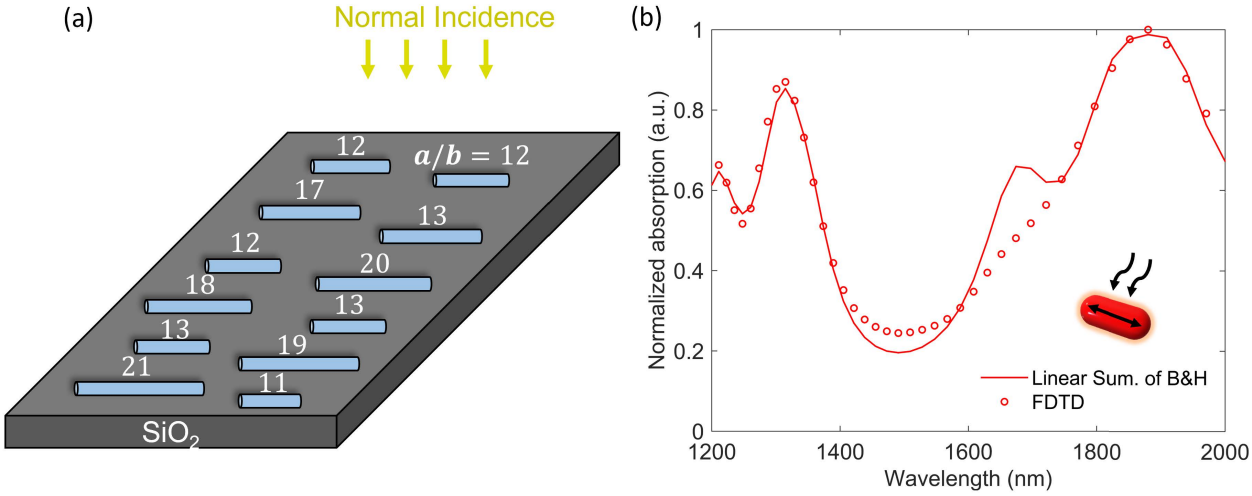

FIGURE 3. A schematic diagram of the optimized nano-chip that consists of 12 silver ellipsoids and SiO_2-based substrate. Particle swarm optimization is used to discover an optimal absorption spectrum where the absorption has multiple peaks except a single transmission window around 1450–1500nm. In order to predict the total absorption spectrum of the ellipsoid array, a single absorption spectrum predicted by the BH model is linearly added up for 12 ellipsoids. (b) The absorption of the optimized nano-chip is validated between the linear summation of the BH model and the numerical simulation result (FDTD).

unity values in the other wavelengths. The PSO algorithm utilizes individual particles to explore an optimum solution through cognitive behavior and social behavior of a bird flock or bees [36]. It has been widely used in solving electromagnetic problems [47], [48] since first introduced by Kennedy and Eberhart. Notably, it is powerful when there is no way to obtain derivatives of a figure of merits. The velocity update equation of the PSO is given by

$$v_i = W \cdot v_i + c_1 \cdot r_1 \cdot (\text{pbest}_i - x_i) + c_2 \cdot r_2 \cdot (\text{gbest}_i - x_i), \tag{10}$$

where v_i is the velocity of the particle in the i_{th} dimension, W means an inertia, c_1 and c_2 are cognitive and social factors, respectively. 'pbest' indicates the location with the best fitness value discovered by a single particle, 'gbest' indicates the location of the best fitness found among whole particles. r_1, r_2 are random number generation functions, x_i is the current location in the i_{th} dimension. The algorithm works as follows: (1) set the locations of each particle, which are the a/b ratio of the silver ellipsoids; (2) evaluate the fitness based on the linear summation of the absorption spectrum computed by the BH model; (3) check the terminate condition; (4) update pbest and gbest; (5) update particle locations and speeds. The PSO iteratively solves the optimization problem with the cognitive and social behavior of the particles. Figure 3(a) shows the optimized silver ellipsoids on the SiO_2 substrate discovered by the PSO algorithm. A few ellipsoids have a/b ratio less than or equal to 13, while the others have a ratio greater than or equal to 17. This implies that the ellipsoids, which have a/b ratio close to 15, may create absorption peaks near 1400–1500nm wavelength. The PSO algorithm also discovered an appropriate number of ellipsoids that create enough absorption spectrum at the non-transparent wavelengths. Figure 3(b) shows the optimized absorption (red curve) obtained from the linear summation of the BH equations; the red dots indicate a simulated absorption, which includes optimized ellipsoids distributed over 1200nm × 300nm × 540nm (W × L × T) size SiO_2 substrate. The substrate is pre-optimized using a multiple reflection theory [49] to create a minimum reflection near 1500nm. The electric field polarization of the incidence wave is intentionally set to match with the long axis of the ellipsoids to create a maximum possible absorption of the optimized nano-chip. The simulated absorption matches well with the analytic prediction, even though the analytic calculation can only predict a single particle response. This reveals that the BH model can be extended for predicting many-particle problems when their spacing is large enough. In the next section, the optimized single nano-chip will be further studied in a more realistic environment.

III. RESULT

The ultimate goal of this work is to design floating nano-chips that create angle-independent transparency at the infrared regime. An optimized single nano-chip was validated at normal incidence in the previous section. Here, we validate the optimized nano-chip for (1) broad incidence angles, and (2) multiple-transmission scenarios. The optimized nano-chip can be applicable to selective electromagnetic shielding, where thousands of nano-chips float over air (or liquid). In this environment, the incidence wave is unpolarized; therefore, ellipsoids strongly interact with the incidence wave when the polarization of the incident wave is close to the ellipsoid's long axis. The optimized silver ellipsoid nano-chip was designed based on the global optimization method [50] combined with an analytic prediction. Then, the

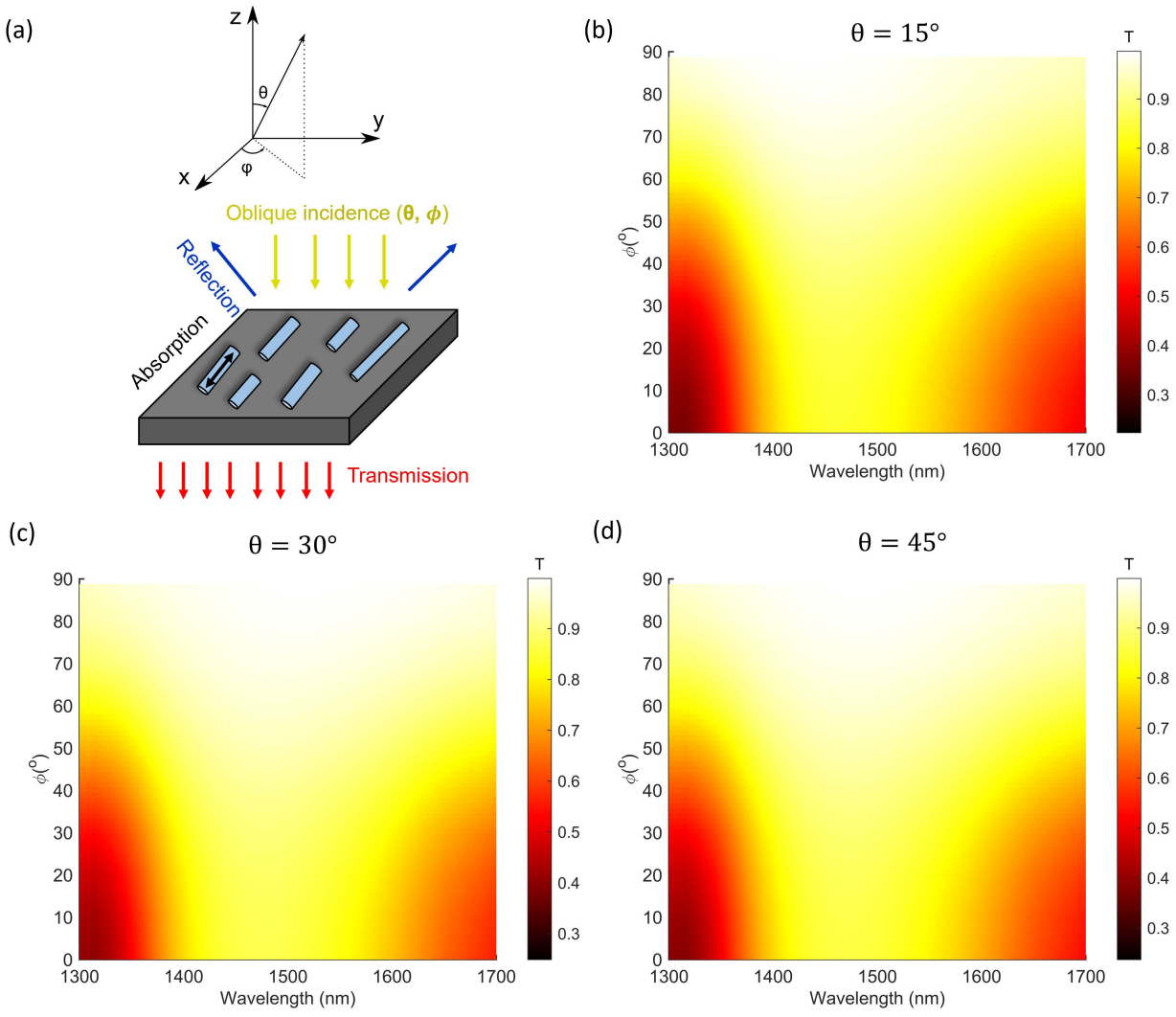

FIGURE 4. (a) A schematic diagram of angle-dependent response of the optimized nano-chip. The incidence angles sweep over θ and ϕ to investigate the angle-dependent response. The optimized nano-chip shows a transparent window between 1450–1500nm wavelength for whole azimuthal and polar angles. (b) $\theta = 15°$, (c) $\theta = 30°$, (d) $\theta = 45°$.

analytic predictions were validated against normal incidence only. In this section, we also numerically study and validate the performance of the optimized floating nano-chips over a broad angle, and broad-wavelength in FDTD. We use perfectly matched layer boundary condition [31], [51] for all directions. 5-nm minimum grid spacing is used with sub-pixel smoothing which greatly improves accuracy of the curved objects [32], [33] in FDTD simulations. The FDTD captures a broad-wavelength response at one simulation with proper time-domain modeling of the dispersive material [52]–[58] (e.g., silver nano-particles in this work). To utilize this advantage, we run multiple simulations with different wavenumbers (k_x, k_y), which represent different oblique incidence angles for different wavelengths. To explore both entire angles and broad wavelength response, we interpolate these simulation results as shown in Fig. 4. The optimized nano-chip creates a transparent window at 1450–1500nm for whole angles (θ, ϕ) for a single transmission scenario. As shown in Fig. 4(b)-(d), the optimized nano-chip does not have a significant θ-dependency due to the cylindrical symmetry of the ellipsoids. The 540-nm-thick SiO_2 substrate has a slight θ-dependent response which could be negligible due to the low absorption coefficient of the SiO_2. We intentionally allow the ϕ-dependent characteristic of the optimized nano-chip because we do not expect to align the polarization of the incidence light with the direction of the ellipsoids in a real environment. However, it is essential to have *ϕ-independenttransparency* at the target wavelengths (1450–1500nm) as validated in Fig. 4(b)-(d). Once we secure this transparency window at the target wavelength, any incidence light (including unpolarized wave) may experience floating nano-chips multiple times. Multiple transmissions may eventually absorb the electromagnetic waves whose wavelength does not match the target wavelengths.

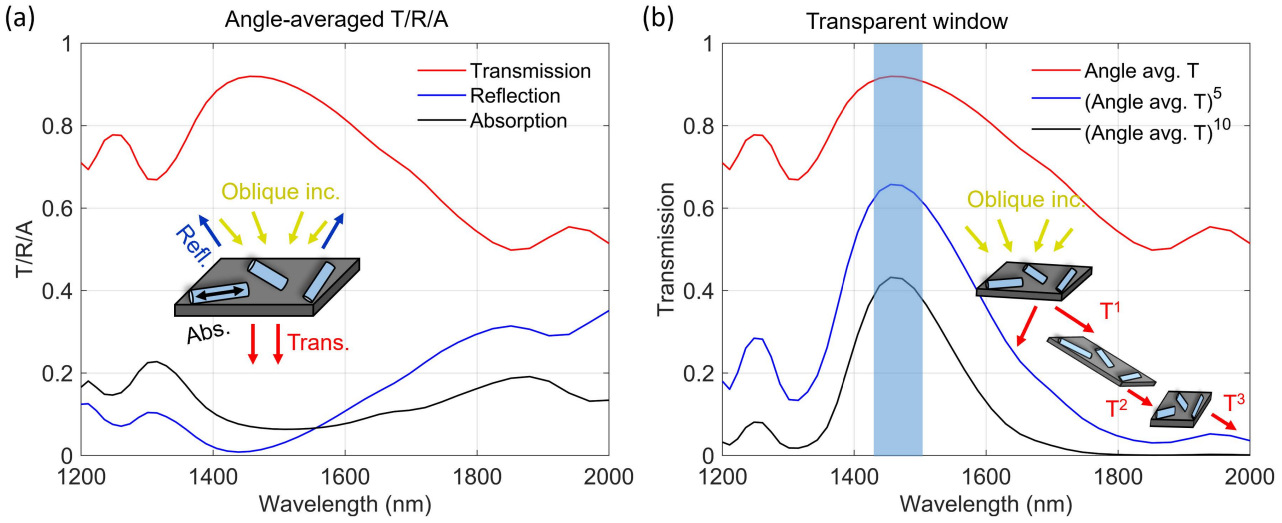

FIGURE 5. (a) Angle-averaged transmission (red curve), reflection (blue curve), and absorption (black curve) spectra of the optimized nano-chip shown in Fig. 3. (b) Incidence waves may experience multiple floating nano-chips in the air (or liquid). The resulting transmission rate of the multiple nano-chip scenarios can be approximated by the power of the transmission calculated for a single nano-chip. The sky-blue area indicates a transparent window between 1450–1500nm wavelength.

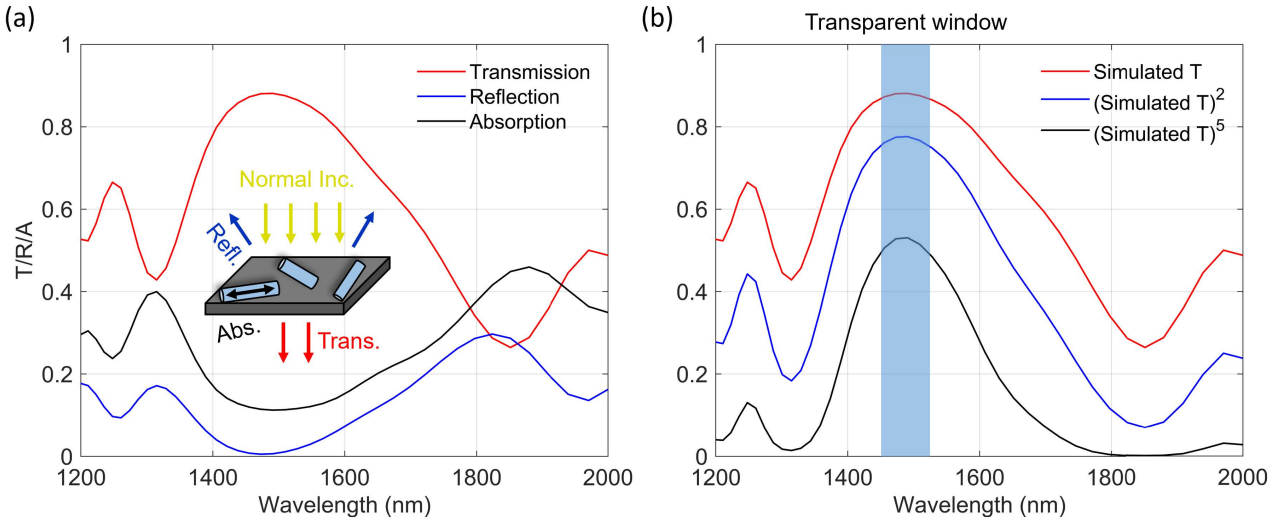

FIGURE 6. (a) Transmission (red curve), reflection (blue curve), and absorption (black curve) spectra of the optimized nano-chip shown in Fig. 3. (b) Incidence waves may experience multiple floating nano-chips in the air (or liquid). The resulting transmission rate of the multiple nano-chip scenarios can be approximated by the power of the transmission calculated for a single nano-chip. The sky-blue area indicates a transparent window between 1450–1500nm wavelength.

Next, we study the optimized nano-chip in a multiple transmission scenario. As shown in Fig. 6, assuming that the optimized nano-chips are floating in air or liquid, we calculate a total transmission of the incident wave. Figure 6(a) shows the transmission, reflection, and absorption of the optimized nano-chip calculated in FDTD with a normal incidence wave. The multiple floating nano-chip scenarios can be approximated by calculating the power of the single transmission, as shown in Fig. 6(b). This scenario is the ideal case where (1) the polarization of the incident wave matches with the long axis of the ellipsoids; (2) the transmitted wave also has the normal incidence angle. We presume that this ideal case is the upper limit of the nano-chip response for $\leq$ 10 transmission events.

A more realistic case would be (1) unpolarized incidence waves, (2) randomly aligned ellipsoids, and (3) unpolarized transmitted waves. We simulate this case by averaging over the broad-angle response and then calculating the power of the averaged transmission as shown in Fig. 5. The angle-averaged response shown in Fig. 5(a) has slightly lower absorption compared with the normal incidence case. This eventually flattens the transmission curve of the multiple

floating nano-chip scenarios shown in Fig. 5(b). However, the transparent characteristic is still maintained at the target wavelength.

IV. CONCLUSION

This work numerically demonstrated floating nano-chips that have electromagnetic transparency in the infrared regime. We proposed a fast optimization strategy that combines global optimization and analytic prediction of the nano-ellipsoid response. The proposed method efficiently discovers a collection of nano-ellipsoids that can block electromagnetic waves that do not fit into the target wavelength regime (1450–1500nm in this work). The optimized floating nano-chip has a 540-nm-thick SiO_2 substrate with 12 silver ellipsoids with a fixed radius of the short axis and different long axes. We numerically validate the angle-dependent characteristic of the nano-chip. Then, in a more realistic case, (1) unpolarized incidence waves, (2) randomly aligned ellipsoids, and (3) unpolarized transmitted waves, have been studied by averaging over the broad-angle response and then calculating the power of the averaged transmission. The optimized nano-chip still maintains electromagnetic transparency in the infrared regime for multiple-transmission, angle-averaged calculations. The proposed strategy can be extended to a long-wavelength infrared regime by utilizing multi-shell nano-particles or different materials. Electromagnetic transparency proposed in this work can be applied to fundamental electromagnetic research and angular-independent spectral filters for 6G communication and battlefield electromagnetic environment.

REFERENCES

[1] N. I. Landy, S. Sajuyigbe, J. J. Mock, D. R. Smith, and W. J. Padilla, "Perfect metamaterial absorber," *Phys. Rev. Lett.*, vol. 100, May 2008, Art. no. 207402.
[2] H.-T. Chen, W. J. Padilla, J. M. O. Zide, A. C. Gossard, A. J. Taylor, and R. D. Averitt, "Active terahertz metamaterial devices," *Nature*, vol. 444, pp. 597–600, Nov. 2006.
[3] C. M. Watts, X. Liu, and W. J. Padilla, "Metamaterial electromagnetic wave absorbers," *Adv. Mater.*, vol. 24, no. 23, pp. OP98–OP120, Jun. 2012.
[4] S. Enoch, G. Tayeb, P. Sabouroux, N. Guérin, and P. Vincent, "A metamaterial for directive emission," *Phys. Rev. Lett.*, vol. 89, no. 21, Nov. 2002, Art. no. 213902.
[5] H. Chung and O. D. Miller, "Tunable metasurface inverse design for 80% switching efficiencies and 144 angular deflection," *ACS Photon.*, vol. 7, no. 8, pp. 2236–2243, 2020.
[6] D. Lin, P. Fan, E. Hasman, and M. L. Brongersma, "Dielectric gradient metasurface optical elements," *Science*, vol. 345, no. 6194, pp. 298–302, 2014.
[7] G. Zheng, H. Mühlenbernd, M. Kenney, G. Li, T. Zentgraf, and S. Zhang, "Metasurface holograms reaching 80% efficiency," *Nature Nanotechnol.*, vol. 10, no. 4, pp. 308–312, Feb. 2015.
[8] X. Ni, A. V. Kildishev, and V. M. Shalaev, "Metasurface holograms for visible light," *Nature Commun.*, vol. 4, no. 1, pp. 1–6, 2013.
[9] M. E. Stewart, C. R. Anderton, L. B. Thompson, J. Maria, S. K. Gray, J. A. Rogers, and R. G. Nuzzo, "Nanostructured plasmonic sensors," *Chem. Rev.*, vol. 108, no. 2, pp. 494–521, Feb. 2008.
[10] S. Linic, P. Christopher, and D. B. Ingram, "Plasmonic-metal nanostructures for efficient conversion of solar to chemical energy," *Nature Mater.*, vol. 10, no. 12, pp. 911–921, Dec. 2011.
[11] B. Luk'yanchuk, N. I. Zheludev, S. A. Maier, N. J. Halas, P. Nordlander, H. Giessen, and C. T. Chong, "The Fano resonance in plasmonic nanostructures and metamaterials," *Nature Mater.*, vol. 9, no. 9, pp. 707–715, Sep. 2010.
[12] H. Chung, K. Jung, and P. Bermel, "Flexible flux plane simulations of parasitic absorption in nanoplasmonic thin-film silicon solar cells," *Opt. Mater. Exp.*, vol. 5, no. 9, pp. 2054–2068, 2015.
[13] H. Wang, D. W. Brandl, F. Le, P. Nordlander, and N. J. Halas, "Nanorice: A hybrid plasmonic nanostructure," *Nano Lett.*, vol. 6, no. 4, pp. 827–832, 2006.
[14] W.-J. Yoon, K.-Y. Jung, J. Liu, T. Duraisamy, R. Revur, F. L. Teixeira, S. Sengupta, and P. R. Berger, "Plasmon-enhanced optical absorption and photocurrent in organic bulk heterojunction photovoltaic devices using self-assembled layer of silver nanoparticles," *Sol. Energy Mater. Sol. Cells*, vol. 94, no. 2, pp. 128–132, Feb. 2010.
[15] K.-Y. Jung, F. L. Teixeira, and R. M. Reano, "Au/SiO_2 nanoring plasmon waveguides at optical communication band," *J. Lightw. Technol.*, vol. 25, no. 9, pp. 2757–2765, Sep. 1, 2007.
[16] T. W. Ebbesen, H. J. Lezec, H. F. Ghaemi, T. Thio, and P. A. Wolf, "Extraordinary optical transmission through sub-wavelength hole arrays," *Nature*, vol. 391, pp. 667–669, Feb. 1998.
[17] L. Martin-Moreno, F. Garcia-Vidal, H. Lezec, K. Pellerin, T. Thio, J. Pendry, and T. and Ebbesen, "Theory of extraordinary optical transmission through subwavelength hole arrays," *Phys. Rev. Lett.*, vol. 86, no. 6, p. 1114, 2001.
[18] H. Liu and P. Lalanne, "Microscopic theory of the extraordinary optical transmission," *Nature*, vol. 452, no. 7188, pp. 728–731, 2008.
[19] Y. Chen, G. Liu, K. Huang, Y. Hu, X. Zhang, and Z. Cai, "Enhanced transmission of a plasmonic ellipsoid array via combining with double continuous metal films," *Opt. Commun.*, vol. 311, pp. 100–106, Jan. 2013.
[20] J.-C. Yan, Z.-K. Li, Y. Zhang, Y.-L. Wang, and C.-P. Huang, "Trapped-mode resonances in all-metallic metasurfaces comprising rectangular-hole dimers with broken symmetry," *J. Appl. Phys.*, vol. 126, no. 21, Dec. 2019, Art. no. 213102.
[21] J. Zhang, W. Bai, L. Cai, Y. Xu, G. Song, and Q. Gan, "Observation of ultra-narrow band plasmon induced transparency based on large-area hybrid plasmon-waveguide systems," *Appl. Phys. Lett.*, vol. 99, no. 18, Oct. 2011, Art. no. 181120.
[22] C. A. Kyriazidou, R. E. Diaz, and N. G. Alexopoulos, "Novel material with narrow-band transparency window in the bulk," *IEEE Trans. Antennas Propag.*, vol. 48, no. 1, pp. 107–116, Jan. 2000.
[23] D.-C. Son, H. Shin, Y. J. Kim, I. P. Hong, H. J. Chun, K.-Y. Jung, H. Choo, and B. Y. Park, "Design of a hemispherical reconfigurable frequency selective surface using water channels," *IEEE Access*, vol. 6, pp. 61445–61451, 2018.
[24] Z. Wu, K. Chen, R. Menz, T. Nagao, and Y. Zheng, "Tunable multiband metasurfaces by moiré nanosphere lithography," *Nanoscale*, vol. 7, no. 48, pp. 20391–20396, 2015.
[25] P.-C. Li and E. T. Yu, "Flexible, low-loss, large-area, wide-angle, wavelength-selective plasmonic multilayer metasurface," *J. Appl. Phys.*, vol. 114, no. 13, Oct. 2013, Art. no. 133104.
[26] H. Tao, C. Bingham, A. Strikwerda, D. Pilon, D. Shrekenhamer, N. Landy, K. Fan, X. Zhang, W. Padilla, and R. Averitt, "Highly flexible wide angle of incidence terahertz metamaterial absorber: Design, fabrication, and characterization," *Phys. Rev. B, Condens. Matter*, vol. 78, no. 24, Dec. 2008, Art. no. 241103.
[27] F. Lotti, A. Mirzaei, A. E. Miroshnichenko, and A. V. Zayats, "Nanoparticle-based metasurfaces for angular independent spectral filtering applications," *J. Appl. Phys.*, vol. 126, no. 21, Dec. 2019, Art. no. 213101.
[28] S. Wu, L. Zhou, Y.-M. Wang, G.-D. Wang, Q.-J. Wang, C.-P. Huang, and Y.-Y. Zhu, "Optical properties of a metal film perforated with coaxial elliptical hole arrays," *Phys. Rev. E, Stat. Phys. Plasmas Fluids Relat. Interdiscip. Top.*, vol. 81, no. 5, May 2010, Art. no. 057601.
[29] J. J. Penninkhof, L. A. Sweatlock, A. Moroz, H. A. Atwater, A. van Blaaderen, and A. Polman, "Optical cavity modes in gold shell colloids," *J. Appl. Phys.*, vol. 103, no. 12, Jun. 2008, Art. no. 123105.
[30] A. Taflove, "Review of the formulation and applications of the finite-difference time-domain method for numerical modeling of electromagnetic wave interactions with arbitrary structures," *Wave Motion*, vol. 10, no. 6, pp. 547–582, 1988.
[31] A. Taflove, S. C. Hagness, and M. Piket-May, *Computational Electromagnetics: The Finite-Difference Time-Domain Method*, vol. 3. Amsterdam, The Netherlands: Elsevier, 2005.
[32] A. F. Oskooi, D. Roundy, M. Ibanescu, P. Bermel, J. D. Joannopoulos, and S. G. Johnson, "Meep: A flexible free-software package for electromagnetic simulations by the FDTD method," *Comput. Phys. Commun.*, vol. 181, no. 3, pp. 687–702, 2010.

[33] A. Farjadpour, D. Roundy, A. Rodriguez, M. Ibanescu, P. Bermel, J. D. Joannopoulos, S. G. Johnson, and G. W. Burr, "Improving accuracy by subpixel smoothing in the finite-difference time domain," *Opt. Lett.*, vol. 31, no. 20, pp. 2972–2974, 2006.
[34] V. E. Do Nascimento, K.-Y. Jung, B.-H. V. Borges, and F. L. Teixeira, "A study on unconditionally stable FDTD methods for the modeling of metamaterials," *J. Lightw. Technol.*, vol. 27, no. 19, pp. 4241–4249, Oct. 1, 2009.
[35] K.-Y. Jung and F. L. Teixeira, "An iterative unconditionally stable LOD–FDTD method," *IEEE Microw. Wireless Compon. Lett.*, vol. 18, no. 2, pp. 76–78, Feb. 2008.
[36] J. Kennedy and R. Eberhart, "Particle swarm optimization," in *Proc. IEEE ICNN*, vol. 4, Nov./Dec. 1995, pp. 1942–1948.
[37] C. F. Bohren and D. R. Huffman, *Absorption Scattering Light by Small Particles*. Hoboken, NJ, USA: Wiley, 2008.
[38] Y. Guo, S. Wang, Y. Zhou, C. Chen, J. Zhu, R. Wang, and Y. Cai, "Broadband absorption enhancement of graphene in the ultraviolet range based on metal-dielectric-metal configuration," *J. Appl. Phys.*, vol. 126, no. 21, Dec. 2019, Art. no. 213103.
[39] S. A. Tretyakov and S. I. Maslovski, "Thin absorbing structure for all incidence angles based on the use of a high-impedance surface," *Microw. Opt. Technol. Lett.*, vol. 38, no. 3, pp. 175–178, Aug. 2003.
[40] J. A. Gordon, C. L. Holloway, and A. Dienstfrey, "A physical explanation of angle-independent reflection and transmission properties of metafilms/metasurfaces," *IEEE Antennas Wireless Propag. Lett.*, vol. 8, pp. 1127–1130, 2009.
[41] K. Wang, J. Zhao, Q. Cheng, D. S. Dong, and T. J. Cui, "Broadband and broad-angle low-scattering metasurface based on hybrid optimization algorithm," *Sci. Rep.*, vol. 4, no. 1, pp. 1–6, May 2015.
[42] Z. Li and K. Aydin, "Broadband metasurfaces for anomalous transmission and spectrum splitting at visible frequencies," *EPJ Appl. MetaMater.*, vol. 2, no. 1, p. 2, 2015.
[43] A. Monti, A. Alù, A. Toscano, and F. Bilotti, "Narrowband transparent absorbers based on ellipsoidal nanoparticles," *Appl. Opt.*, vol. 56, no. 27, pp. 7533–7538, 2017.
[44] J. Dai, F. Ye, Y. Chen, M. Muhammed, M. Qiu, and M. Yan, "Light absorber based on nano-spheres on a substrate reflector," *Opt. Exp.*, vol. 21, no. 6, pp. 6697–6706, 2013.
[45] H. Ni, M. Wang, H. Hao, and J. Zhou, "Integration of tunable two-dimensional nanostructures on a chip by an improved nanosphere lithography method," *Nanotechnology*, vol. 27, no. 22, Jun. 2016, Art. no. 225301.
[46] E. D. Palik, *Handbook of Optical Constants of Solids*, vol. 3. New York, NY, USA: Academic, 1998.
[47] G. Ciuprina, D. Ioan, and I. Munteanu, "Use of intelligent-particle swarm optimization in electromagnetics," *IEEE Trans. Magn.*, vol. 38, no. 2, pp. 1037–1040, Mar. 2002.
[48] J. Robinson and Y. Rahmat-Samii, "Particle swarm optimization in electromagnetics," *IEEE Trans. Antennas Propag.*, vol. 52, no. 2, pp. 397–407, Feb. 2004.
[49] H. Chung, K.-Y. Jung, X. T. Tee, and P. Bermel, "Time domain simulation of tandem silicon solar cells with optimal textured light trapping enabled by the quadratic complex rational function," *Opt. Exp.*, vol. 22, no. S3, p. A818, 2014.
[50] H. Choo, A. Hutani, L. C. Trintinalia, and H. Ling, "Shape optimisation of broadband microstrip antennas using genetic algorithm," *Electron. Lett.*, vol. 36, no. 25, pp. 2057–2058, Dec. 2000.
[51] S. Jang and K.-Y. Jung, "Perfectly matched layer formulation of the INBC-FDTD algorithm for electromagnetic analysis of thin film materials," *IEEE Access*, vol. 9, pp. 118099–118106, 2021.
[52] H. Chung, J. Cho, S.-G. Ha, S. Ju, and K.-Y. Jung, "Accurate FDTD dispersive modeling for concrete materials," *ETRI J.*, vol. 35, no. 5, pp. 915–918, Oct. 2013.
[53] H. Chung and O. D. Miller, "High-NA achromatic metalenses by inverse design," *Opt. Exp.*, vol. 28, no. 5, pp. 6945–6965, 2020.
[54] C. Kim, J. Heo, K.-Y. Jung, H. Choo, and Y. B. Park, "Propagation from geostationary orbit satellite to ground station considering dispersive and inhomogeneous atmospheric environments," *IEEE Access*, vol. 8, pp. 161542–161550, 2020.
[55] H. Choi, Y.-H. Kim, J.-W. Baek, and K.-Y. Jung, "Accurate and efficient finite-difference time-domain simulation compared with CCPR model for complex dispersive media," *IEEE Access*, vol. 7, pp. 160498–160505, 2019.
[56] J.-W. Baek, D.-K. Kim, and K.-Y. Jung, "Finite-difference time-domain modeling for electromagnetic wave analysis of human voxel model at millimeter-wave frequencies," *IEEE Access*, vol. 7, pp. 3635–3643, 2019.
[57] S.-G. Ha, J. Cho, E.-K. Kim, Y. B. Park, and K.-Y. Jung, "FDTD dispersive modeling with high-order rational constitutive parameters," *IEEE Trans. Antennas Propag.*, vol. 63, no. 9, pp. 4233–4238, Sep. 2015.
[58] S.-M. Park, E.-K. Kim, Y. B. Park, S. Ju, and K.-Y. Jung, "Parallel dispersive FDTD method based on the quadratic complex rational function," *IEEE Antennas Wireless Propag. Lett.*, vol. 15, pp. 425–428, 2016.

JUNJEONG PARK received the B.S. degree in electrical engineering from Soongsil University, Seoul, South Korea, in 2021, where he is currently pursuing the M.S. degree in developing inverse design algorithm for novel metasurfaces. His research interests include design, analysis, and optimization of metasurfaces, which are applied in imaging, biosensors, and AR/VR devices.

SUN K. HONG (Senior Member, IEEE) received the B.S. degree in electrical engineering from the University of Maryland, College Park, MD, USA, in 2005, and the M.S. and Ph.D. degrees in electrical engineering from Virginia Tech, Blacksburg, VA, USA, in 2008 and 2012, respectively. From 2005 to 2015, he was a Research Engineer with the U.S. Naval Research Laboratory. From 2015 to 2017, he was an Assistant Professor with the Department of Electrical and Computer Engineering, Rose-Hulman Institute of Technology, Terre Haute, IN, USA. In 2017, he joined the School of Electronic Engineering, Soongsil University, Seoul, where he is currently an Assistant Professor. His current research interests include wireless power transfer, electromagnetic waves in complex environments, detection of nonlinear devices, radars, and high-power electromagnetics.

HAEJUN CHUNG received the B.S. degree *(magna cum laude)* in electrical engineering from the Illinois Institute of Technology, Chicago, USA, in 2011, the degree in electrical engineering from Hanyang University, Seoul, South Korea, in 2012, and the M.S. and Ph.D. degrees in electrical and computer engineering from Purdue University, IN, USA, in 2013 and 2017, respectively. He joined as a Postdoctoral Research Associate in applied physics at Yale University, CT, USA, in 2017. Then, he joined as a Postdoctoral Research Associate in mechanical engineering at the Massachusetts Institute of Technology, MA, USA, in 2020. He joined Soongsil University, Seoul, in 2021, where he is currently an Assistant Professor at the School of Electrical Engineering. His main research interests include a fast inverse design algorithm, novel metasurfaces, metalenses, biosensors, and photovoltaics.